arXiv:hep-ex/0106041v2   9 Jun 2001

Studying the ω-mass in-medium in $\gamma + A \to \pi^0 \gamma + X$ reactions

J.G. Messchendorp[1], A. Sibirtsev[2,3], W. Cassing[2], V. Metag[1], S. Schadmand[1]

[1] II. Physikalisches Institut, Universität Gießen, 35392 Gießen, Germany
[2] Institut für Theoretische Physik, Universität Gießen, 35392 Gießen, Germany
[3] Institut für Kernphysik, Forschungszentrum Jülich GmbH, 52425 Jülich, Germany

Abstract. Simulations based on a coupled-channel transport model have been performed to analyze the feasibility to study the in-medium ω mass exploiting the process $\gamma + A \to \pi^0 \gamma + X$ for C, Ca and Nb nuclei. The distortions due to final-state interactions of the π^0 and background contributions from the reaction $\gamma + A \to \pi^0 \pi^0 + X$ are found to be small in the mass range of interest ($0.6 < M_{\pi^0 \gamma} < 0.8$ GeV).

Furthermore, the effect of the detector resolution on the $\pi^0 \gamma$-mass determination is discussed.

PACS. 13.60.-r Photon and charged-lepton interactions with hadrons – 13.60.Le Meson production – 25.20.-x Photonuclear reactions – 14.40.-n Mesons

1 Introduction

The modification of hadron properties in the nuclear medium is one of the current topics in hadron and nuclear physics. Vector-meson properties in the nuclear medium have attracted considerable attention since their in-medium spectral function was measured by dilepton spectroscopy ($l^+ l^-$) without distortion due to final-state interactions. An enhancement in the lepton pair spectrum from heavy-ion collisions relative to proton-nucleus reactions has been observed by the CERES [1,2,3] and HELIOS-3 [4] collaborations at the SPS in the invariant-mass range from 0.4 – 0.7 GeV. As proposed in Refs. [5, 6,7,8,9] an enhancement can be understood in terms of a modification of the vector-meson properties in dense and hot nuclear matter. Collisional broadening of the ρ-meson width or dropping of the ρ-mass pole might be responsible for the experimental observations. The in-medium modifications of vector mesons have also been discussed in Refs [10,11,12,13,14] in the context of photo-absorption data on nuclei [11,15]. Recently, it was suggested [16] that photoproduction data can provide access to the momentum dependence of the in-medium ρ-meson potential [17, 18,19].

Theoretical studies within different models predict a dropping of the in-medium ρ-meson mass (m^*) at normal nuclear-matter density ($\rho_0 = 0.16$ fm^{-3}) within the range of $-240 \leq m^* - m_V \leq -45$ MeV [20,21,22,23,24,25,26], where m_V denotes the bare ρ-mass. However, it was argued in Refs. [27,28,29,30,31] that due to substantial collisional broadening the ρ-meson might not survive as a "proper" quasiparticle at large nuclear densities and only reflects

a continuum spectral strength of the isovector current. Thus, the ρ-meson spectral function is difficult to identify at high baryon density.

The situation is better for the ω-meson. Here, the predictions for a modification of the ω-mass (at normal nuclear-matter density ρ_o) are within the range $-140 \leq m^* - m_V \leq -15$ MeV [25,31,32,33,34,35], while the ω-meson collisional width is estimated within the range of 20 to 50 MeV [31,32,36]. Thus it is expected that the in-medium ω-meson survives as a quasiparticle and can be observed as a structure in the ω-mass spectrum. In this case, one should observe a significant resonance structure on top of a continuum.

The ϕ and J/Ψ mesons should also change their masses slightly at normal nuclear density with a small collisional width due to the almost negligible interaction with nucleons [22,23,25,31]. However, their in-medium modifications are rather small compared to the ω-meson and their production is suppressed due to the internal $s\bar{s}$ or $c\bar{c}$ quark structure.

In heavy-ion collisions the baryon density varies dramatically with time due to the formation and expansion of the "fireball". It was proposed in Refs. [38,39,40,41,44, 45,46,47,48] to study the in-medium vector meson properties in the interactions of pions, protons or photons with nuclei. Both the $l^+ l^-$ and $\pi^0 \gamma$ invariant-mass spectra have been discussed as possibilities investigating the vector-meson properties in matter.

Only vector mesons decaying inside nuclei can be used for an identification of the in-medium properties. This imposes the kinematic condition [49] that the decay length of the vector meson $L_V \propto E_V / m_V \Gamma_V$ should be less than the nuclear radius. It implies that the vector mesons should be

produced at small velocities or energies E_V from heavy-nuclear targets. Furthermore, because of the finite vector-meson life time, $1/\Gamma_V$, only a fraction will decay inside the nucleus and the final spectra will show the signal from decays inside and outside the target nucleus as well as contributions from the interference of the two amplitudes.

In case of dilepton measurements in γA reactions [41] the in-medium signal from ω-meson decays is superimposed on a broad signal from the ρ-meson. In addition, the dilepton measurements in γA reactions are dominated by the Bethe-Heitler process, which can only be suppressed by rather severe kinematic cuts [41]. Therefore, the $\pi^0\gamma$ measurements appear to be more promising.

The in-medium properties of vector mesons can be detected with dilepton spectroscopy as mentioned above. As was proposed in Refs. [37,38], an alternative way to study the in-medium modification of the ω-meson is to look at the $\omega \rightarrow \pi^0 + \gamma$ decay mode. This mode accounts for $8.5 \cdot 10^{-2}$ of the total ω decay width, while for the ρ-meson it is only $6.8 \cdot 10^{-4}$. The contribution of the ρ-meson to the $\pi^0\gamma$-mass distribution is therefore negligible, which makes the $\pi^0\gamma$-decay mode an exclusive probe to study the ω-meson properties in matter.

It should be pointed out that the reconstruction of the $\omega \rightarrow \pi^0 + \gamma$ mode is hindered by the final-state interactions of the π^0-meson in the nucleus, which might be quite strong in case of large nuclei [38]. In addition, the pion from the ω decay may be off-shell, too. Furthermore, the finite experimental efficiency causes a mis-identification of four γ events from the channels $\pi^0\pi^0$, $\eta\pi^0$ and related reactions with more than three photons in the final channel. Thus the $\pi^0\gamma \rightarrow 3\gamma$ mode requires a full understanding of the contributions from these reactions.

We investigate the possibility to deduce the in-medium modification of the ω-meson from the $\pi^0\gamma$ invariant-mass distribution for $\gamma+A$ reactions and evaluate the optimal experimental conditions for the photon energy and the size of the target nucleus. We will apply kinematic cuts on 3 photon events in order to identify the distortion of the in-medium signal due to the π^0-meson final state interaction. Our study is designed for the TAPS [42] and Crystal Barrel [43] experiment at ELSA. The detector response is known and the background contribution due to the final-state mis-identifications, caused by the detector efficiency and the corrections due to the experimental resolution in the reconstruction of the $\pi^0\gamma$ spectrum, are calculated.

2 Ingredients of the model

The calculations were performed within the transport model previously applied to ρ, K^+, K^- and ω meson production in pion-nucleus and proton-nucleus collisions [38, 45,50]. In the following, we describe the new ingredients of the model relevant to photoproduction of ω-mesons and the calculation of the background $\gamma+N\rightarrow\pi^0+\pi^0+N$ reaction.

In Fig. 1, the $\gamma+p\rightarrow\omega+p$ cross section is shown as a function of the photon energy E_γ from Ref. [51]. The

dashed line gives the result for the ω cross section calculated within the π and η-meson exchange model where the parameters have been adopted from Refs. [53,54]. Our calculations are close to the predictions of Refs. [53,54]. The discrepancy between the data and the calculations at $E_\gamma \geq 2.5$ GeV might be due to additional contributions from pomeron exchange [54], which plays a dominant role at high energies [55].

For an application in our transport calculations we parameterize the data on the $\gamma+p \rightarrow \omega+p$ cross section as

$$\sigma = \frac{[(s-m_N^2-m_\omega^2)^2-4m_N^2m_\omega^2]^{1/2}}{s\,(s-m_N^2)} \frac{A}{(\sqrt{s}-M)^2+\Gamma^2/4}, \quad (1)$$

where s, m_N and m_ω are the squared invariant collision energy, the nucleon and ω-meson masses, respectively. The parameters M=1.7 GeV, Γ=6 GeV and A=396 μb$\cdot$GeV^{-4} have been fitted to the data [51].

The solid line in Fig. 1 shows the parametrization (1) that reproduces the available data [51] reasonable well. We mention that the parameterization (1) is also in agreement with recent SAPHIR data [56,57]. The cross section on the neutron was taken to be the same as on a proton.
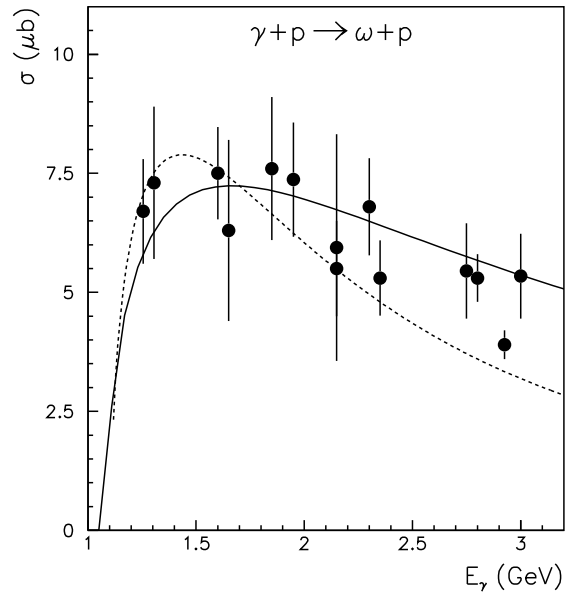

Fig. 1. The ω-meson photoproduction cross section on the proton as a function of the photon energy. The experimental data are taken from Ref. [51]. The solid line shows the parameterization (1), while the dashed line corresponds to a calculation within the π- and η-meson exchange model [53,54].

In the transport code the ω-mesons are produced in accordance with their spectral function. In addition to the vacuum spectral function, an in-medium modification was introduced by the real and imaginary part of an effective ω-meson potential [38]

$$\Re U_\omega(\rho) = m_\omega \ \beta \ \frac{\rho}{\rho_0},$$

$$\Im U_\omega(\rho) = \Gamma_{coll}\, \frac{\rho}{\rho_0}, \qquad (2)$$

where m_ω is the bare ω-meson mass, ρ_0=0.16 fm^{-3} and ρ is the local nuclear density. The parameter β=–0.16 was adopted from the model predictions in Refs. [25,31, 32,33,34,35] and the collisional width Γ_{coll}=50 MeV was taken from Refs. [31,36]. We calculate the production, the propagation and decay of the ω-meson inside the potential (2). This prescription consistently guarantees that the ω-mesons decaying outside the nuclei regain the ω-spectral function in vacuum.

The linear-density approximation in Eq. (2) is in reasonable agreement[1] with the density dependence of the real part of the vector-meson potential calculated in Refs. [24,58] for finite nuclei.

Furthermore, we account for the elastic and inelastic ω-meson interactions in nuclei employing the cross sections given in Ref. [36]. We calculate the distortion of the $\omega \to \pi^0\gamma$ signal due to the re-scattering of the π^0-meson by adopting the total and elastic $\pi+N$ differential cross sections from the Karlsruhe-Helsinki partial-wave analysis [59,60]. In the medium, however, many-body phenomena like two-nucleon absorption of pions may occur additionally, which is very pronounced for low momentum pions [61], but becomes questionable for pion momenta above 350 MeV/c since the pion wavelength must be somewhat larger than the average distance between nucleons. We have investigated the role of such many-body effects by calculating π^+ absorption on nuclei for pion momenta above 300 MeV/c employing the cross sections from [59, 60]. As a genuine result we find that for ^{65}Fe and ^{209}Bi nuclei we overestimate the pion absorption by 10-20 %, respectively, in comparison to the data from Ref. [62]. This result is fully in line with the earlier transport studies by Engel et al. in Ref. [63]. In addition, we have analyzed the two-nucleon absorption in the ω-production channel discussed in this paper. For the energies presented here, the effect of an additional two-nucleon absorption is estimated to be around 5%. We thus discard additional many-body phenomena in order not to overestimate the π^0 reabsorption.

To calculate the background from two neutral pions we implement the elementary photoproduction cross section shown in Fig. 2. While data [51] for the $\gamma+p\to\pi^++\pi^-+p$ cross section are available for a large range of photon energies, data for the $\gamma+p\to\pi^0+\pi^0+p$ reaction are only available up to $E_\gamma \simeq$0.8 GeV [52]. We employ a resonance model to construct a parameterization over the desirable range of photon energies. As shown by the dashed lines in Fig. 2, the contribution from the baryonic resonances coupled to two pions can be calculated for both reactions by taking into account the resonance properties from the analysis in Ref. [64]. We assume the same energy dependence of the non-resonant contribution for the $\gamma+p\to\pi^0+\pi^0+p$ and the $\gamma+p\to\pi^++\pi^-+p$ reaction, however, scale the strength in line with the low-energy data [52]. Our estimate for the

---

[1] For instance, the comparison between the scaling [5,20] and the calculations [24,58] for a carbon target is shown in Fig. 3 of Ref. [50].
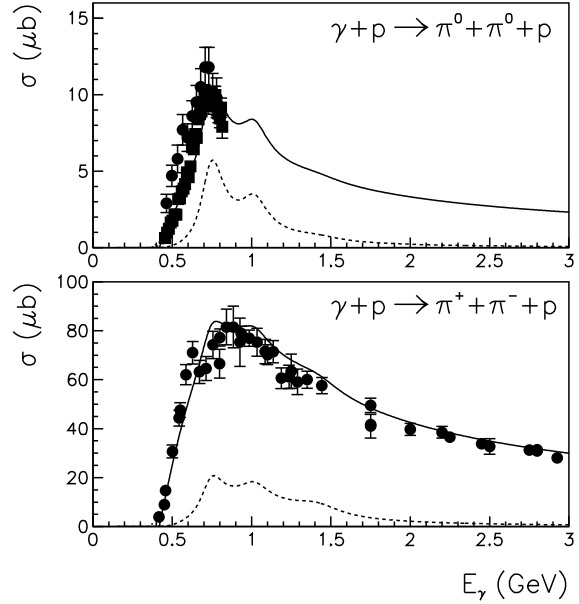

Fig. 2. The $\gamma+p\to\pi^0+\pi^0+p$ and $\gamma+p\to\pi^++\pi^-+p$ cross sections as a function of the photon energy. The experimental data are taken from Refs. [52,51]. The solid lines show our parameterization, while the dashed lines indicate the contribution from the baryonic resonances.

$\gamma+p\to\pi^0+\pi^0+p$ cross section is in reasonable agreement with the microscopic calculations of Ref. [65].

Experimental data on the $\gamma+N\to\eta+\pi^0+N$ reaction, that might contribute to the background, are not available. We thus discard this channel in our present calculations. It is known experimentally [51] that the total $\gamma+N$ cross section is almost saturated by the sum of the $\gamma+N\to\pi+N$, $\gamma+N\to2\pi+N$ and $\gamma+N\to\eta+N$ partial cross sections below a photon energy of 1.3 GeV. At higher photon energies the dominant contributions to the total $\gamma+N$ cross section stem from multi-pion production [51].

Since not only the ω-meson, but also the decay pion changes its spectral function in the medium, the in-medium ω Dalitz decay has to be discussed explicitly. Now let the in-medium ω mass be M and the decay pion have a mass m_π^* that is selected by Monte Carlo according to its in-medium width Γ_π^* and mass shift δm_π. Energy and momentum conservation - in the rest frame of the ω meson - than implies

$$M^2 = (E_\pi^* + E_\gamma)^2 = (\sqrt{p_\pi^{*2} + m_\pi^{*2}} + E_\gamma)^2, \qquad (3)$$

with $E_\gamma = |p_\pi^*|$ denoting the photon energy which in magnitude equals the momentum of the decay pion. Whereas the photon propagates to the vacuum without distortion, the in-medium pion changes its momentum and spectral function during the propagation to the vacuum according to quantum off-shell propagation [66,67]. In the particular case, where the pion self energy Σ_π has no explicit time dependence ($\partial_t\Sigma_\pi = 0$) and is only a function of momentum and density, which holds well for the case of $p + A$ reactions, the energy of the pion $E_\pi^* = E_\pi$ is a constant of motion (cf. Eq. (20) in Ref. [67]). Thus the off-shell

mass and momentum balance out during the propagation as shown graphically in Ref. [67] in Figs. 1 and 2 for a related problem. The magnitude of the pion momentum in vacuum - if not scattered explicitly or being absorbed - then is given by

$$p_\pi^v = \sqrt{p_\pi^{*2} + m_\pi^{*2} - m_0^2}, \qquad (4)$$

where m_0 denotes the vacuum pion mass and p_π^* the pion momentum in the ω decay in-medium. The invariant mass (squared) of the pion and photon in the vacuum then is given by

$$M_r^2 = (E_\pi + E_\gamma)^2 - (p_\pi^v - E_\gamma)^2 = M^2 - (p_\pi^v - E_\gamma)^2. \quad (5)$$

The pion propagation thus leads to a slight downward shift of the invariant mass in vacuum relative to its original in-medium value. We note, that the above considerations apply well for heavy nuclei where the corrections in energy due to the recoil momentum of the nucleus ($|p_\pi^v - E_\gamma|$) can be discarded.
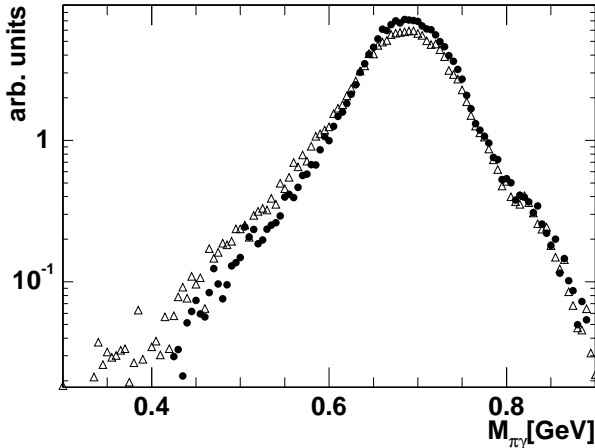

Fig. 3. A BUU Monte-Carlo prediction of the in-medium $\pi^0 \gamma$ mass distribution for the reaction $\gamma + Ca \to \pi^0 \gamma + X$ at an incident photon energy of 1.2 GeV. The effect of the mean-field interaction of the π^0 with the nucleus is studied by comparing the prediction of an unmodified π^0 meson (filled circles) and the prediction for which the π^0 mass is modified according to a Breit-Wigner distribution with a width of 150 MeV (open triangles).

For an actual quantification of this effect one has to specify the pion spectral function e.g. at nuclear matter density ρ_0. The pions, that originate from the ω decay in $\gamma + A$ reactions, have typical momenta ≥ 300 MeV such that their interaction cross section with nucleons is in the order of 30-35 mb, while their velocity β_π relative to the target is close to 1. Consequently the collisional broadening can be estimated as

$$\delta\Gamma_\pi \approx \beta_\pi \sigma_{\pi N} \rho_0 \approx 85 - 120 \; MeV, \qquad (6)$$

which is still quite substantial. For a test case we have assumed the ω in-medium spectral function to be represented by a Breit-Wigner of width $\Gamma_{tot} = 50$ MeV and

pole mass of 0.65 GeV. Then for each invariant mass M the decay of the ω to a photon and an in-medium pion can be evaluated and the pion momentum p_π^v according to (4). The results of the simulations for the pion off-shell effects on the reconstructed invariant mass distribution in (5) show that for a pion collisional broadening of 100 – 200 MeV the shift in invariant mass is practically invisible at the pole mass and only becomes more pronounced in the low mass tails of the invariant mass distribution. In Fig. 3 the π^0 off-shell effect is displayed quantitatively for the reaction $\gamma + Ca \to \pi^0 \gamma + X$ at an incident photon energy of 1.2 GeV. Shown is the $\pi^0 \gamma$-mass distribution for those ω mesons which decay inside the nucleus. Indicated are the distributions assuming freely propagating on-shell π^0 mesons (filled circles) and assuming a modification of the π^0 spectral function by a Breit-Wigner distribution with a width of Γ=150 MeV (open triangles). As seen from Fig. 3, the mean-field propagation of the π^0 meson in the nucleus can be safely neglected especially in view of presently achievable experimental mass resolutions (see Section 4). Furthermore, the spectrum is strongly distorted by π^0 rescattering only in the low mass tails (see Section 3.2). Thus we continue our studies with on-shell calculations for the pions without substantial loss in accuracy.

3 Model predictions

The coupled-channel transport model described in the previous section has been adopted in a Monte-Carlo simulation to examine and optimize the feasibility of measuring the ω mass at nuclear densities in the process $\gamma + A \to \pi^0 \gamma + X$. In particular, the effect of the final-state π^0 rescattering to the ω-mass determination is studied. Furthermore, the dependence on the incident photon energy and the atomic mass of the nucleus is addressed in this section. In sections 4 and 5 the effect of experimental resolution and background processes are discussed.

3.1 Incident photon energy

The fraction of ω mesons decaying inside the nucleus can be optimized by minimizing the decay length $L_\omega \propto E_\omega / m_\omega \Gamma_\omega$. It is therefore preferred that the kinetic energy of the ω meson is small. This can be achieved with an incident photon energy close to the ω-production threshold as illustrated in Fig. 4. Here, the kinetic-energy distributions of the ω produced in the reaction $\gamma + Ca \to \omega + X$ for an incident photon energy of E_γ=1.2 GeV (solid histogram) and an incident photon energy of E_γ=2.0 GeV (dotted histogram) are compared. Clearly, the ω meson has the smallest average energy for E_γ=1.2 GeV. Furthermore, at E_γ=1.2 GeV the ω-production cross section is still comparable to the cross sections at larger incident photon energies (see Fig. 1). Thus in the simulations described below an incident photon energy of E_γ=1.2 GeV is used.
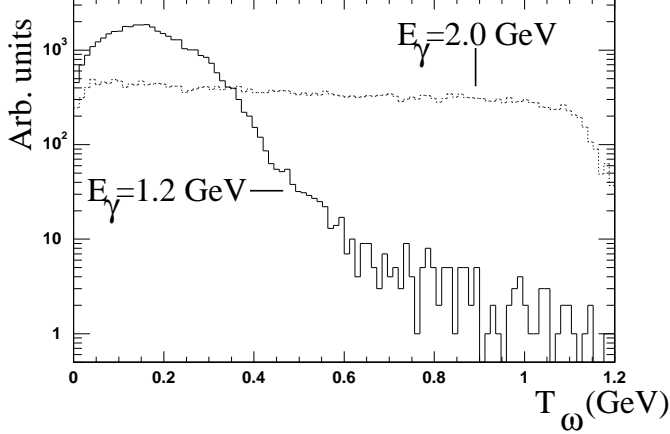
Fig. 4. The kinetic-energy distributions of the ω meson in the reaction $\gamma + Ca \rightarrow \omega + X$ for incident photon energies of E_γ=1.2 GeV (solid histogram) and E_γ=2.0 GeV (dotted histogram).

3.2 π^0 rescattering

One of the critical arguments against studying the ω-mass in-medium by the decay $\omega \rightarrow \pi^0\gamma$ is the strong final-state interaction of the π^0. The transport model allows to study this effect quantitatively. In Fig. 5 this is illustrated for the reaction $\gamma + Nb \rightarrow \pi^0\gamma + X$ at E_γ=1.2 GeV. The figure shows the $\pi^0\gamma$-mass distribution decomposed in the fraction of ω mesons decaying outside the nucleus (**a**), the fraction decaying inside the nucleus (**b**) (for which the π^0 does not rescatter) and the fraction decaying inside the nucleus in case of π^0 rescattering (**c**). Note, that a fraction of approximately 36% of the ω mesons decays inside the nucleus. By definition, a particle decays "inside" the nucleus if the density $\rho > 0.05$ fm^{-3}. A shift (of $\approx$20%) and the effect of collisional broadening (of $\approx$50 MeV) of the ω-mass distribution can be observed as parametrized according to Eqs. (2). For $\approx$40% of all the ω mesons decaying inside the nucleus, the final-state π^0 does rescatter. However, this background appears dominantly at relatively small invariant masses $M_{\pi^0\gamma}$ and is spread out over a large mass range. The scattering of the π^0 with the nucleons alter its direction and kinetic energy such that the initial ω-mass information is essentially lost. Hence, the π^0-rescattering contribution is significantly smaller in the range 0.6< $M_{\pi^0\gamma}$ <0.8 GeV than the contribution of ω mesons decaying inside without π^0 rescattering.

The energy loss of the rescattered π^0 mesons can be exploited experimentally to reduce the background from rescattering even further. This is illustrated in Fig. 6, showing the $\pi^0\gamma$-mass distribution versus the reconstructed kinetic energy of the π^0. Clearly, the contribution of ω mesons decaying inside the nucleus - with π^0 rescattering - is correlated with low-energy π^0. Without a significant loss of the actual signal (ω mesons decaying inside the medium without rescattering of the π^0), the dominant part of the π^0-rescattering background can
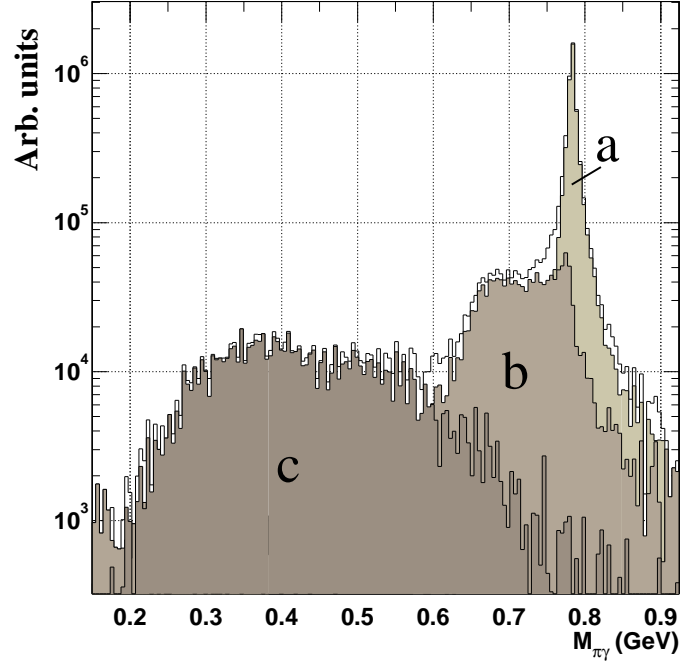

Fig. 5. The $\pi^0\gamma$-mass distribution obtained from a Monte-Carlo simulation of the process $\gamma + Nb \rightarrow \pi^0\gamma + X$ at E_γ=1.2 GeV. The spectrum is decomposed into different contributions corresponding to the fraction of ω mesons decaying outside ($\rho < 0.05$ fm^{-3}) the nucleus (**a**), the fraction of ω mesons decaying inside ($\rho > 0.05$ fm^{-3}) for which the π^0 does not rescatter (**b**), and the fraction of ω mesons decaying inside the nucleus for which π^0 rescatters (**c**).

be eliminated by selecting π^0 mesons with a kinetic energy $T_{\pi^0} > 150$ MeV. The resulting $\pi^0\gamma$-mass distribution is shown in Fig. 7. An improvement compared to Fig. 5 can be observed. The contribution of the π^0-rescattering background is now reduced to 1% within the mass range of $0.6 < M_{\pi^0\gamma} < 0.8$ GeV. Besides exploiting the energy loss of the rescattered π^0, angular correlations between the incident photon, the final-state photon and the π^0 meson can be used to enhance the in-medium signal relative to π^0-rescattering background. An analysis has shown that a similar result as shown in Fig. 7 can be obtained by alternatively gating on the opening angle between the final-state π^0 and γ and cutting on the out-of-plane angle of the π^0 relative to the incident and final-state γ-γ plane.

3.3 Atomic-mass dependence

The dependence of the ω-mass in-medium on the atomic mass (A) has been studied by performing Monte-Carlo simulations for different nuclei. The result is shown in Fig. 8 for a proton, carbon, calcium and niobium target, varying A between 1 and 92. All spectra are normalized at the pole mass of the ω ($M_{\pi^0\gamma}$=0.78 GeV). Obviously, the contribution of the ω mesons decaying inside the nucleus
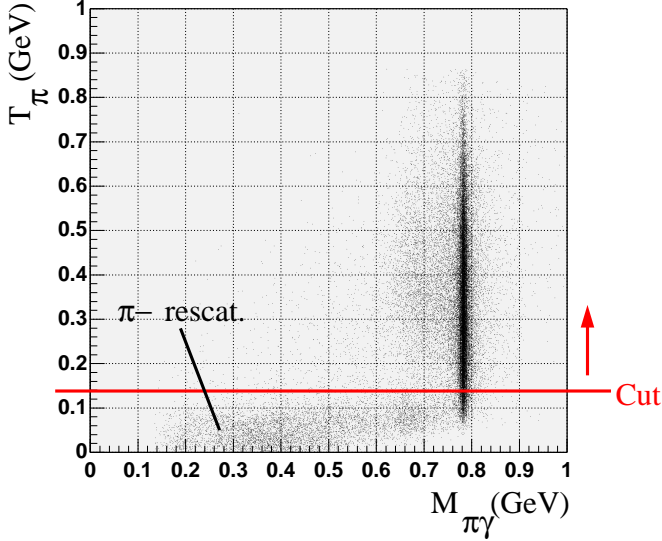
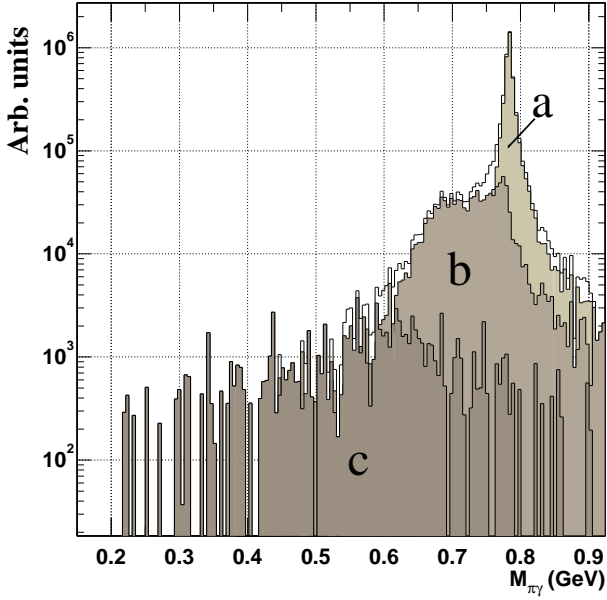**Fig. 6.** The $\pi^0\gamma$-mass distribution versus the reconstructed kinetic energy of the final-state π^0.

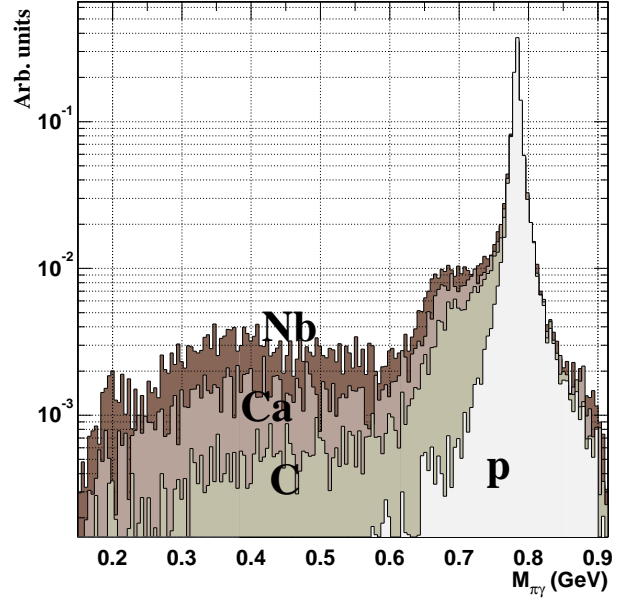**Fig. 7.** The same as Fig. 5 with the additional condition of $T_{\pi^0} > 150$ MeV.

Fig. 8. The $\pi^0\gamma$-mass distribution as predicted by the coupled-channel transport model for $\gamma + A \to \pi^0\gamma + X$ at E_γ=1.2 GeV and A=p, C, Ca and Nb. The spectra are normalized at the ω peak $M_{\pi^0\gamma}$=0.78 GeV.

Table 1. The fraction of ω mesons decaying outside the nucleus, inside the nucleus (i.e. at $\rho > 0.3\,\rho_0$) with and without π^0 rescattering for carbon, calcium and niobium. The effect of an additional cut on $T_{\pi^0} >$150 MeV is shown as the values within brackets. All values are given in percentage of the total ω-production rate.

Nucleus	Decay outside	Decay inside without π^0 rescattering	Decay inside with π^0 rescattering
C (A=12)	83.7 (86.1)	13.4 (13.3)	2.8 (0.62)
Ca (A=40)	73.8 (80.4)	18.4 (18.4)	7.8 (1.2)
Nb (A=92)	65.0 (75.7)	21.5 (22.0)	13.5 (2.3)

tering, and inside the nucleus with π^0 rescattering. In addition, the effect of a cut on $T_{\pi^0} > 150$ MeV is included in the table (values in brackets).

4 Experimental resolution

A realistic simulation has to take the effect of a finite detector resolution on the $\pi^0\gamma$-mass determination into account. Therefore, we have included in the simulation a photon position resolution of σ=1.2° and a photon energy response as measured with the photon spectrometer TAPS consisting of BaF$_2$ crystals [42]. A similar resolution is expected for the Crystal Barrel detector (CsI) [43], therefore providing a realistic simulation for future experiments at ELSA. The effect on the invariant-mass determination for different nuclei is shown in Fig. 9. Although an obvious
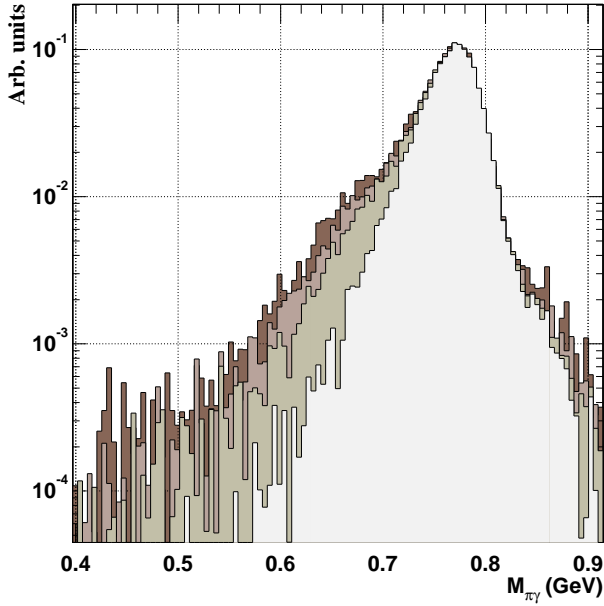
(with and without π^0 rescattering) increases as function of A simply due to an increase in the effective radius of the nucleus. One might argue that a larger nucleus, like Pb, is more suited. However, for heavy targets one has to take into account the decrease in radiation length with Z^2, therefore increasing the fraction of incident photons converting into a lepton pair. In Table 1 we have summarized a quantitative analysis of the different contributions for different targets, e.g. the fraction of ω mesons decaying outside the nucleus, inside the nucleus without π^0 rescat-

Fig. 9. The $\pi^0\gamma$-mass distribution corresponding to Fig. 8 for p, C, Ca, Nb including the effect of a realistic detector resolution. Furthermore, a cut on the kinetic energy of the pion of $T_{\pi^0} >$150 MeV is applied.

Fig. 10. The $\pi^0\gamma$-mass distribution as expected for $\gamma + Nb$ at an incident photon energy of 1.2 GeV. The contribution from the background channel $\gamma + Nb \rightarrow \pi^0\pi^0 + X$ is indicated as grey area. The probability of not detecting a photon is assumed to be 5%. Furthermore, the detector response is included and a cut on $T_{\pi^0} > 150$ MeV is applied.

decrease in the mass resolution can be observed by a comparison with Fig. 8, a shoulder due to ω mesons decaying inside the nucleus is still visible and increases with the size of the nucleus. The figure demonstrates the necessity of measuring the $\pi^0\gamma$ mass for a set of different targets to avoid experimental ambiguities.

5 Channel misinterpretation

So far, the effect of experimental background has not been considered in the simulations. We expect the main source of background to come from a misidentification of the $\gamma + A \rightarrow \pi^0\gamma + X$ reaction due to not detecting one of the photons of the process $\gamma + A \rightarrow \pi^0\pi^0 + X$. Therefore, the latter reaction has been implemented in the calculation as described in section 2 and simulated in the same framework as the $\gamma + A \rightarrow \pi^0\gamma + X$ process. The result for $\gamma + Nb$ at an incident photon energy of 1.2 GeV is shown in Fig. 10. Here, we assumed that the probability of not detecting a photon due to detector thresholds, inefficiencies and acceptances is 5%. The contribution of the $\pi^0\pi^0$ background as indicated by the shaded part of the spectrum is $\approx$36% of the total yield. In the mass range of interest ($0.6 < M_{\gamma\pi^0} < 0.8$ GeV) the contribution is only 1%.

The fraction of the $\pi^0\pi^0$ background to the total mass distribution can be reduced by simple kinematic cuts as proposed in Fig. 11. In this figure, the energy distribution of one of the photons of the $\gamma + Nb \rightarrow \pi^0\pi^0 + X$ reaction (grey line) is compared to the energy distribu-
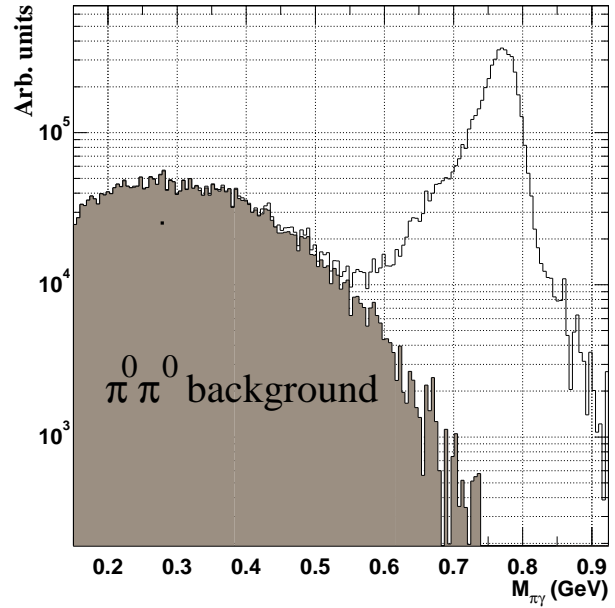
tion of the photon of the $\gamma + Nb \rightarrow \pi^0\gamma + X$ reaction (solid line). Clearly, requiring the photon energy to be larger than 200 MeV reduces the $\pi^0\pi^0$ background significantly without a large loss of the actual signal. The effect of an additional cut of $E_\gamma > 200$ MeV on the $M_{\pi^0\gamma}$ distribution is shown in Fig. 12 for $\gamma + Nb$ at an incident photon energy of 1.2 GeV. In addition, the contribution of ω mesons decaying outside the nucleus and the contribution decaying inside the nucleus, with and without π^0 rescattering, are depicted. Note that the background from π^0 rescattering and from the $\pi^0\pi^0$ channel within the complete mass range between $M_{\pi^0\gamma}$=0.6 and 0.8 GeV is significantly smaller than the signal of interest, i.e. the fraction of ω mesons decaying inside without a rescattering of the π^0.

6 Conclusions

In this study the feasibility of measuring the ω spectral function at normal nuclear densities is discussed by exploiting the process $\gamma + A \rightarrow \pi^0\gamma + X$. Experimentally, this process will be studied with the Crystal Barrel detector [43] at ELSA in coincidence with the photon spectrometer TAPS [42]. Such experiments are complementary to plans at GSI and CEBAF to measure the channels $\pi^- + A \rightarrow e^+e^- + X$ and $\gamma + A \rightarrow e^+e^- + X$ with the HADES [68] and CLAS [69] detector, respectively. The processes are sensitive to the spectral functions of
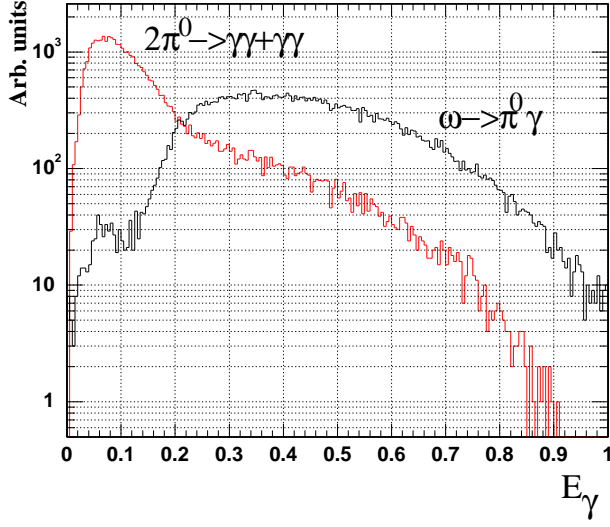
Fig. 11. The energy distributions of the photons (that do not correspond to one of the decay products of the pion) from the $\gamma + Nb \rightarrow \pi^0 \gamma + X$ channel is compared with the energy distribution of photons from the $\gamma + Nb \rightarrow \pi^0 \pi^0 + X$ channel.
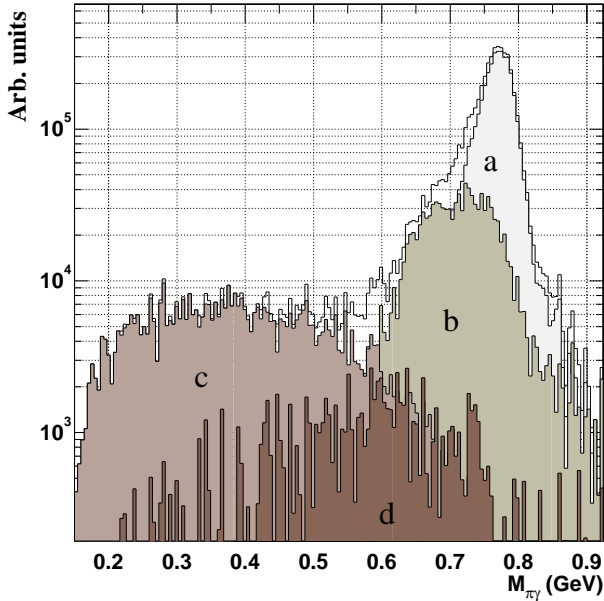

Fig. 12. The $\pi^0 \gamma$-mass distribution for $\gamma + Nb$ at an incident photon energy of 1.2 GeV. The fraction of ω mesons decaying outside the nucleus (**a**), inside the nucleus without π^0 rescattering (**b**), inside the nucleus with π^0 rescattering (**d**) and the background from the $2\pi^0$ (**c**) are indicated. The experimental resolution is taken into account. Furthermore, kinematical cuts to reduce the background from π^0 rescattering and from the $2\pi^0$ channel have been applied (see text).

the ρ-meson, which has a large decay branch into $e^+ e^-$ pairs. Furthermore, photon-induced dilepton studies have to take into account the contribution from the dominant Bethe-Heitler process.

The main drawback of measuring the ω mass in-medium via its decay $\omega \rightarrow \pi^0 \gamma$ is the use of a hadronic probe (π^0) which has a sizeable probability to interact with the nucleons. The influence of this background on the mass determination has been studied using a coupled-channel transport calculation adopted in a Monte-Carlo simulation. Although the final-state interactions of the π^0 meson are found to be large, its contribution at the invariant mass region of interest $(0.6 < M_{\pi^0 \gamma} < 0.8$ MeV) is small. A kinematic cut on the kinetic energy of the π^0 allows for a further reduction of the π^0-rescattering background, leading to an almost negligible contribution to the $\pi^0 \gamma$ invariant-mass distribution.

The photon spectrometers, TAPS and Crystal Barrel, have a finite mass resolution which is larger than the decay width of a free-propagating ω meson. This hinders the observation of an in-medium mass shift of the ω meson. Simulations including a realistic $\pi^0 \gamma$-mass resolution show that within the assumption of a mass reduction according to Brown-Rho scaling [5] and an additional increase in the decay width due to collisional broadening of $\Gamma_{coll} \approx 50$ MeV, a shift in the ω mass can still be experimentally observed. In particular, differences in the $\pi^0 \gamma$ invariant-mass spectrum for several nuclei might provide evidence for a mass shift.

The dominant experimental background is expected to stem from the process $\gamma + A \rightarrow \pi^0 \pi^0 + X$. By missing one of the photons, this channel can be misidentified as a $\gamma + A \rightarrow \pi^0 \gamma + X$ reaction. This background has been estimated using the coupled-channel model, and it is found to be small at the $\pi^0 \gamma$-mass region where a mass shift of the ω meson is expected. Kinematic cuts on the energy of the photons have demonstrated to be an efficient technique to reduce this source of contamination.

In conclusion, it is shown that the $\gamma + A \rightarrow \pi^0 \gamma$ process can be used experimentally to measure the in-medium mass of the ω meson. This conclusion is based upon assumptions on properties of the in-medium ω meson, like mass and width, which theoretically are considered to be realistic.

Acknowledgements

References

1. G. Agakichiev et al., Phys. Rev. Lett. **175**, (1995) 1272.
2. G. Agakichiev et al., Phys. Lett. B **422**, (1998) 405.
3. G. Agakichiev et al., Nucl. Phys. **661**, (1999) 23.
4. M. Masera et al., Nucl. Phys. A **590**, (1992) 93.
5. G.E. Brown and M. Rho, Phys. Rev. Lett. **66**, (1991) 2720.

6. G.Q. Li, C.M. Ko and G.E. Brown, Phys. Rev. Lett. **75**, (1995) 4007.

7. W. Cassing, W. Ehehalt and C.M. Ko, Phys. Lett. B **363** (1995) 35.

8. R. Rapp, G. Chanfray and J. Wambach, Nucl. Phys. A **617**, (1997) 472.

9. W. Cassing and E.L. Bratkovskaya, Phys. Rep. **308**, (1999) 65.

10. S. Boffi, Ye. Golubeva, L.A. Kondratyuk and M.I. Krivoruchenko, Nucl. Phys. A **606**, (1996) 421.

11. N. Bianchi, E. De Sanctis, M. Mirazita and V. Muccifora, Phys. Rev. C **60**, (1999) 064617.

12. R. Rapp, M. Urban, M. Buballa and J. Wambach, Phys. Lett. B **417**, (1998) 1.

13. V. Muccifora et al., Phys. Rev. C **60**, (1999) 064616.

14. R. Rapp and J. Wambach, hep-ph/9909229.

15. N. Bianchi et al., Phys. Rev. C **54**, (1996) 1688.

16. T. Falter, S. Leupold and U. Mosel, Phys. Rev. C **62**, (2000) 031602.

17. V.L. Eletsky and B.L. Ioffe, Phys. Rev. Lett. **78**, (1997) 1010.

18. L.A. Kondratyuk, A. Sibirtsev, W. Cassing, Ye.S. Golubeva and M. Effenberger, Phys. Rev. C **58**, (1998) 1078.

19. V.L. Eletsky, B.L. Ioffe and J.I. Kapusta, Eur. Phys.J. A **3**, (1998) 381.

20. T. Hatsuda and S.H. Lee, Phys. Rev. C **46**, (1992) 34.

21. M. Asakawa and C.M. Ko, Phys. Rev. C **48**, (1993) 526.

22. Y. Koike, Phys. Rev. C **51**, (1995) 1488.

23. X. Jin and D. Leinweber, Phys. Rev. C **52**, (1995) 3344.

24. K. Saito, K. Tsushima and A.W. Thomas, Phys. Rev. C **56**, (1997) 566.

25. K. Tsushima, D.H. Lu, A.W. Thomas and K. Saito, Phys. Lett. B **443**, (1998) 26.

26. S. Leupold, W. Peters and U. Mosel, Nucl. Phys. A **628**, (1998) 311.

27. G. Chanfray and P. Schuck, Nucl. Phys. A **555**, (1993) 329.

28. M. Herrmann, B. Friman and W. Nörenberg, Nucl. Phys. A **560**, (1993) 411.

29. R. Rapp, G. Chanfray and J. Wambach, Phys. Rev. Lett. **76**, (1996) 368.

30. B. Friman and H.J. Pirner, Nucl. Phys. A **617**, (1997) 496.

31. F. Klingl, N. Kaiser and W. Weise, Nucl. Phys. A **624**, (1997) 527.

32. B. Friman, Acta Phys. Pol. B **29**, (1998) 3115.

33. K. Saito, K. Tsushima, A.W. Thomas and A.G. Williams, Phys. Lett. B **433**, (1998) 243.

34. K. Saito, K. Tsushima, D.H. Lu and A.W. Thomas Phys. Rev. C **59**, (1999) 1203.

35. F. Klingl, T. Waas and W. Weise, Nucl. Phys. A **650**, (1999) 299.

36. G.I. Lykasov, W. Cassing, A. Sibirtsev and M.V. Rzyanin, Eur. Phys. J. A **6**, (1999) 71.

37. Ye.S. Golubeva et al., Eur. Phys. J. A **7**, (2000) 271.

38. A. Sibirtsev, V. Hejny, H. Ströher and W. Cassing, Phys. Lett. B **483**, (2000) 405.

39. Th. Weidmann, E.L. Bratkovskaya, W. Cassing and U. Mosel, Phys. Rev. C **59**, (1999) 919.

40. M. Effenberger, E.L. Bratkovskaya, W. Cassing and U. Mosel, Phys. Rev. C **60**, (1999) 027601

41. M. Effenberger, E.L. Bratkovskaya and U. Mosel Phys. Rev. C **60**, (1999) 044614.

42. A.R. Gabler et al., Nucl. Instr. and Meth. A **346**, (1994) 168.

43. E. Aker et al., Nucl. Instr. and Methods A **321**, (1992) 69.

44. Ye.S. Golubeva, L.A. Kondratuyk and W. Cassing, Nucl. Phys. A **625**, (1997) 832.

45. A. Sibirtsev and W. Cassing, Nucl. Phys. A **641**, (1998) 476.

46. W. Schön et al., Acta Phys. Pol. B **27**, (1996) 2954.

47. V. Metag, πN-Newsletter **11**, (1995) 159.

48. V. Metag, Nucl. Phys. A **630**, (1998) 1c.

49. N.N. Nikolaev, J. Speth and B.G. Zakharov, Phys. Atom. Nucl. **63**, (2000) 1463.

50. A. Sibirtsev and W. Cassing, Nucl. Phys. A **629**, (1998) 717.

51. Landolt-Börnstein, New Series **I/12**, ed. H. Schopper, Springer-Verlag, (1998).

52. M. Wolf et al., European Journal of Physics A, (2000) in print.

53. B. Friman and M. Soyeur, Nucl. Phys. A **600**, (1996) 477.

54. Y. Oh, A.I. Titov and T.S.H. Lee, nucl-th/0004055.

55. A. Donnachie and P.V. Landshoff, Phys. Lett. B **478**, (2000) 146.

56. F. J. Klein et al., πN Newslett. **14**, (1998) 141.

57. F. Klein, Prog. Part. Nucl. Phys. **44**, (2000) 159.

58. K. Tsushima, private communication.

59. G. Höhler, Pion-Nucleon-Scattering, Landolt-Börnstein, **/I/9**, Springer-Verlag, (1993.

60. R. Koch, Z. Phys. C **29**, (1985) 597.

61. T. Ericson and W. Weise, *Pions in Nuclei*, Clarendon Press, Oxford 1988.

62. D. Ashery et al., Phys. Rev. C **23**, (1981) 503.

63. A. Engel, W. Cassing, U. Mosel, M. Schäfer and Gy. Wolf, Nucl. Phys. A **572**, (1994) 657.

64. D.M. Manley, R.A. Arndt, Y. Goradia and V.L. Teplitz, Phys. Rev. D **30**, (1984) 904.

65. J.A. Gomez Tejedor and E. Oset, Nucl. Phys. A **600**, (1996) 413.

66. W. Cassing and S. Juchem, Nucl. Phys. A **665**, (2000) 377; A **677**, (2000) 445.

67. W. Cassing and S. Juchem, Nucl. Phys. A **672**, (2000) 417.

68. J. Friese et al. (HADES collaboration), Prog. Part. Nucl. Phys. **42** (1999) 235.

69. M.V. Kossov et al., Program Advisory Committee report PR 94-002 (1994).